

Quantum-number-projected generator coordinate method and the shell model

K. Enami, K. Tanabe, and N. Yoshinaga

Department of Physics, Saitama University, Saitama City 338-8570, Japan

(Received 8 February 2002; published 29 May 2002)

The validity of the quantum-number-projected generator coordinate method (PGCM) is investigated within the proton-neutron single- j shell model. The results of the PGCM are compared with exact solutions in the shell model. It is concluded that the PGCM provides a good approximation of the shell model for low-lying collective states. In order to describe the proton-neutron relative motion such as a scissors mode, we also propose a truncation scheme in terms of the PGCM. Various classes of PGCM truncations are examined by changing sets of generator coordinates. Flexibility with respect to the choice of generator coordinates is advantageous to illuminate the underlying physics. As an application of the PGCM truncation, the $M1/E2$ transition probabilities concerning the $I=1^+$ scissors state are analyzed for nuclei exhibiting stable triaxiality. The electromagnetic properties are identified. Those are characteristic of the $O(6)$ dynamical symmetry limit of the proton-neutron interacting boson model.

DOI: 10.1103/PhysRevC.65.064308

PACS number(s): 21.10.Re, 21.60.Cs

I. INTRODUCTION

The single- j shell model has been widely utilized as a testing ground for many microscopic theories [1–6]. Its great simplicity allows us to obtain exact solutions and to sweep away any ambiguity arising from the numerical analysis. The quantal effect is strongly amplified in small systems such as the single- j shell model. This feature is also suitable for investigating a fully quantal theory, which goes beyond the mean-field approximation. The model contains enough physical contents to judge the effectiveness of a theoretical method.

In our consecutive papers [7–10], the capability of the quantum-number-projected generator coordinate method (PGCM) was investigated within the single- j shell model of identical nucleons. The PGCM was proved to be an excellent approximation of the shell model, irrespective of the shell fillings. It was also clarified that the projected potential energy surface (PPES) offers an intuitive insight into shell model spectra [7]. Furthermore, we demonstrated the capability of the PGCM to reproduce the change of spectroscopic properties accompanied by shape evolution from the sphere to the maximal deformation [8]. The PGCM combined with the study of the PPES leads to some unexpected outcomes, such as stable triaxiality in the ground state, which cannot be predicted within the mean-field approximation.

The purpose of this paper is to test the validity of the PGCM in a more realistic situation, i.e., the proton-neutron single- j shell model. This work completes our studies of the PGCM within the single- j shell model. We examine various kinds of PGCM's by changing the choice of generator coordinates. The analysis based on the PGCM is classified roughly into two schemes. One constructs the total system from the single PGCM state, and the other from the angular momentum coupling of the proton and neutron PGCM states. In the former scheme, total spin I is projected out directly from a product wave function of the mean-field theory. The PGCM levels derived directly from the Hill-Wheeler equation are compared with exact solutions in the shell model. In the latter scheme, the PGCM is used to truncate the exact

shell model configuration space in each proton or neutron system. The proton and neutron parts are treated separately in the PGCM stage, and they are coupled through the diagonalization of the total Hamiltonian.

In Sec. II the model Hamiltonian and intrinsic states are given. We introduce three systems investigated in the present work. In Sec. III the PGCM scheme is directly applied to the simulation of exact spectra. In Sec. IV the shell model configuration space is truncated by various kinds of PGCM's. In analyzing numerical results, we pay much attention to the PPES. In Sec. V electromagnetic properties concerning the $I=1^+$ scissors mode are examined, in connection with the proton-neutron interacting boson model. We conclude the paper in Sec. VI.

II. HAMILTONIAN, INTRINSIC STATE, AND MODEL NUCLEI

In this paper, we investigate a model where protons and neutrons in each single- j shell interact through pure quadrupole-quadrupole interaction (QQI),

$$\hat{H} = \hat{H}_\pi + \hat{H}_\nu + \hat{H}_{\pi\nu},$$

$$\hat{H}_\pi + \hat{H}_\nu = -\frac{1}{2} \sum_{\tau=\pi,\nu} \sum_{\mu=-2}^2 \chi_{\tau\tau} \hat{Q}_\mu^{(\tau)\dagger} \hat{Q}_\mu^{(\tau)}, \quad (1)$$

$$\hat{H}_{\pi\nu} = -\chi_{\pi\nu} \sum_{\mu=-2}^2 \hat{Q}_\mu^{(\nu)\dagger} \hat{Q}_\mu^{(\pi)},$$

where the subscripts π and ν indicate protons and neutrons, and $\hat{Q}_\mu^{(\tau)}$ ($\tau=\pi$ or ν) denotes the dimensionless mass quadrupole operator, the definition of which is given in Refs. [7], [9]. A common force parameter is assumed, i.e., $\chi = \chi_{\pi\pi} = \chi_{\nu\nu} = \chi_{\pi\nu} = 1$ (MeV), except when we compare the strength of the p - n QQI component with that of the identical nucleon components.

Intrinsic states of protons and neutrons, $|\Phi_\pi\rangle$ and $|\Phi_\nu\rangle$, are determined from the Nilsson or Nilsson BCS model

[7–11]. The total intrinsic state, which is employed as the generating function of the PGCM, is given by their product $|\Phi\rangle=|\Phi_\pi\rangle|\Phi_\nu\rangle$. In the Nilsson scheme, we assume the common potential deformation (β, γ) for both protons and neutrons.

It is characteristic of the single- j shell model that the Nilsson intrinsic state reaches the maximum deformation as soon as the potential deformation is switched on [11]. The Nilsson state does not depend on β , so that γ becomes the only parameter specifying the intrinsic state. Thus, the allowed deformation for the model nucleus is strictly restricted, unless the pairing correlation exists [7]. In order to stress this property, we use the term “*deformation limit*” for the deformed Nilsson states, in accordance with our previous work [8]. The Nilsson intrinsic state is expressed as $|\Phi(\gamma)\rangle [=|\Phi_\pi(\gamma)\rangle|\Phi_\nu(\gamma)\rangle]$ hereafter.

By applying the BCS scheme to Nilsson single-particle levels, better generating functions are provided. In the present work, the significance of the pairing correlation lies in the expansion of the deformation region [8], since our model Hamiltonian does not contain the pairing interaction. The single- j shell is such a small system that the deformation of the model nucleus quickly reaches its upper limit as β increases. In order to specify the extent of deformation in a unique manner, we introduce intrinsic quantities $\mathbf{q}=(q_0, q_2)$ and $\mathbf{q}_\tau=(q_{0\tau}, q_{2\tau})$ in terms of the expectation values of the quadrupole operators

$$q_0=q_{0\pi}+q_{0\nu}, \quad q_2=q_{2\pi}+q_{2\nu} \quad (2)$$

with definitions

$$q_{0\tau}=\langle\Phi_\tau|\hat{Q}_0^{(\tau)}|\Phi_\tau\rangle, \quad q_{2\tau}=-\sqrt{2}\langle\Phi_\tau|\hat{Q}_2^{(\tau)}|\Phi_\tau\rangle. \quad (3)$$

It is noted that \mathbf{q}_τ does not fluctuate for a fixed \mathbf{q} ($=\mathbf{q}_\pi+\mathbf{q}_\nu$), since protons and neutrons share the same potential deformation (β, γ) . We express the Nilsson BCS intrinsic state as $|\Phi(\mathbf{q})\rangle [=|\Phi_\pi(\mathbf{q}_\pi)\rangle|\Phi_\nu(\mathbf{q}_\nu)\rangle]$ hereafter.

In the present paper, we focus on the following three model nuclei labeled A , B , and C , which are typical of the p - n single- j shell model. The values of j ($j=j_\pi=j_\nu$) and the neutron and proton numbers (N, Z) for each system are summarized as

$$\begin{aligned} A, \quad j &= \frac{13}{2}, \quad (N, Z) = (10, 10), \\ B, \quad j &= \frac{13}{2}, \quad (N, Z) = (4, 10), \\ C, \quad j &= \frac{11}{2}, \quad (N, Z) = (6, 6). \end{aligned} \quad (4)$$

In Figs. 1(a–c), we show the ground-state PPES’s for the three systems, which result from simultaneous spin- and particle-number projections. All the possible shapes allowed for the system are represented by the coordinates in the q_0 - q_2 plane. For system A , both proton and neutron mean fields favor the prolate distribution. As a consequence of the

spin projection, the system possesses a small triaxial shape. The prominent minimum of the PPES appears at $\gamma=30^\circ$ for systems B and C . The triaxiality-favoring tendency is not an unusual feature in the single- j shell model, provided that the spin projection is taken into account. The potential energy is lowered with increasing deformation. The minimum of the PPES is realized at a point where the pairing gap is almost zero for system B , and exactly zero (deformation limit) for systems A and C . This is due to a manifest property of the QQI. The good agreement between the minimum of the PPES and the exact ground-state energy justifies the predicted equilibrium shape.

III. STANDARD PGCM

In the mean-field theory, the superfluid deformed state is described by the spontaneous breakdown of the gauge and rotational symmetries, which must be conserved in the finite nucleus. Neither total spin I and its z component M nor the nucleon numbers N and Z are good quantum numbers for the Nilsson BCS state. The eigenstate of I , M , N , and Z can be extracted from such an intrinsic state by means of the quantum-number-projection method. A linear superposition of many projected wave functions labeled by generator coordinates set up the PGCM wave function. Depending on the objectives, suitable generator coordinates are incorporated into the PGCM wave function. In the present model, the most general PGCM wave function for the κ th state of spin I is given by

$$|\Psi_{I\kappa MNZ}\rangle = \int d\mathbf{q} \sum_{K=-I}^I \mathcal{F}_{KK}^{INZ}(\mathbf{q}) \hat{P}_{MK}^I \hat{P}^N \hat{P}^Z |\Phi(\mathbf{q})\rangle, \quad (5)$$

where \hat{P}_{MK}^I is the spin projection operator, and \hat{P}^N and \hat{P}^Z are the neutron and proton number projection operators, respectively. The positive parity is always ensured as a good quantum number for all the states appearing in the present paper. The weight functions $\mathcal{F}_{KK}^{INZ}(\mathbf{q})$ and the PGCM energies $E_{I\kappa}$ are determined by solving the Hill-Wheeler equation

$$\begin{aligned} \int d\mathbf{q}' \sum_{K'=-I}^I \{ \langle\Phi(\mathbf{q})|\hat{H}_{KK'}^I \hat{P}^N \hat{P}^Z |\Phi(\mathbf{q}')\rangle \\ - E_{I\kappa} \langle\Phi(\mathbf{q})|\hat{P}_{KK'}^I \hat{P}^N \hat{P}^Z |\Phi(\mathbf{q}')\rangle \} \mathcal{F}_{K'\kappa}^{INZ}(\mathbf{q}') = 0 \end{aligned} \quad (6)$$

under the normalization condition

$$\langle\Psi_{I\kappa MNZ}|\Psi_{I'\kappa' M' N' Z'}\rangle = \delta_{I, I'} \delta_{\kappa, \kappa'} \delta_{M, M'} \delta_{N, N'} \delta_{Z, Z'}. \quad (7)$$

In the numerical analysis, PGCM levels calculated up to spin $I=8$ are compared with exact solutions in the shell model. Detailed accounts of the numerical analysis have been given in Refs. [7–9].

Judging from the functional behavior of the ground-state PPES shown in Fig. 1, we can expect that intrinsic states in the deformation limit provide suitable generating functions of the PGCM. First, we examine the PGCM in the deformation limit. In this case, the twofold integral concerning \mathbf{q}

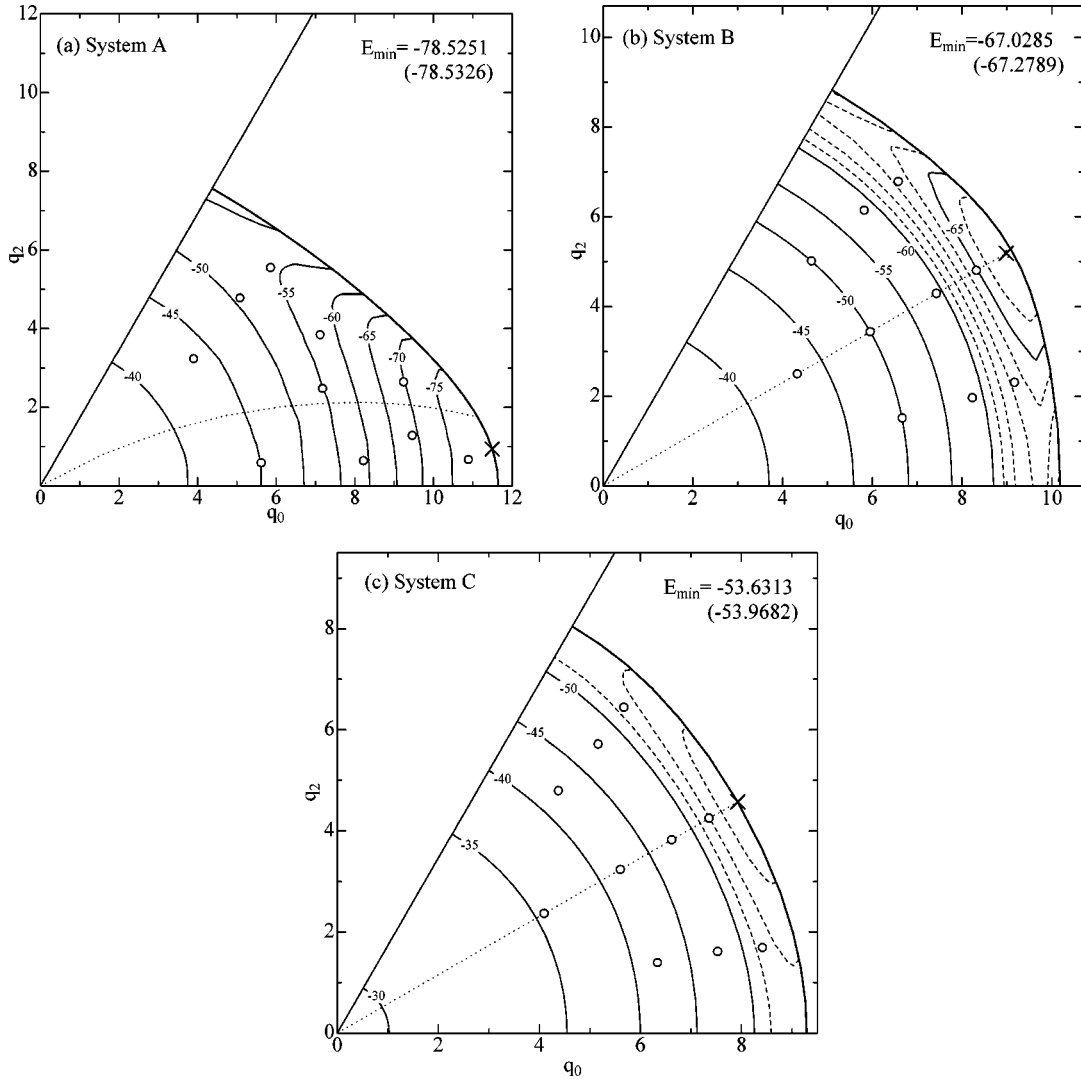


FIG. 1. Contour plots of the ground-state PPES's for the systems A (a), B (b), and C (c). The contour line separation is 5 MeV. Some auxiliary contour lines indicated by dashed lines with a separation energy of 1 MeV are added for the systems B and C. Dotted line corresponds to potential deformation with $\gamma=30^\circ$. The point where the potential energy takes its minimum is indicated by a cross, and its value is shown in the figure. For comparison, the exact ground-state energy of the shell model calculation is also given in parentheses. The placement of ten deformation points taken in the PGCM2 calculation (cf. Sec. III) is indicated by open circles.

$=(q_0, q_2)$ can be replaced with the single γ integral, and the nucleon number projections can be dropped. Second, we proceed to the more desirable PGCM given in Eq. (5), the deformation region of which is extended to the full q_0 - q_2 plane. In order to distinguish two PGCM schemes, we call the former PGCM1 and the latter PGCM2.

Numerical results for the three systems are shown in Figs. 2–4. In the left panel, the PPES's in the deformation limit are plotted as functions of γ . The maximum number of the spin projected levels up to $I=8$ is limited to 21 due to the D_2 symmetry assumed in the intrinsic state. For systems B and C, all the 21 PPES's are displayed in the figure. In the right panel, level schemes of two PGCM's and the shell model are compared. In the PGCM1, deformation points are taken along the curved line corresponding to the deformation limit. We arrange 21 points at regular intervals ($\Delta\gamma=3^\circ$) from $\gamma=0^\circ$ to 60° . The effect of the configuration mixing concern-

ing γ can be estimated by the direct comparison between the levels in the PGCM1 and the PPES's. The calculation of the PGCM2 is carried out by taking 31 deformation points. We add ten deformation points to the 21 points in the PGCM1. The placement of the additional ten points is indicated by open circles in Figs. 1(a–c). The numerical analysis of the PGCM2 is much more elaborate than that of the PGCM1, since it necessitates the particle-number projection in 520 PGCM kernels out of 961 ($=31\times31$) ones.

We recognize some features in these figures. To begin with, we pay attention to the PPES. System A shows simple band structure, typical of well deformed nuclei. This indicates that the intrinsic state is not strongly affected by the collective motion. The intrinsic states with $\gamma=0^\circ\sim30^\circ$ generate similar projected levels. This outcome is explained by Fig. 1(a), from which we find that the correspondence between γ and $\tan^{-1}(q_2/q_0)$ is not good in the deformation

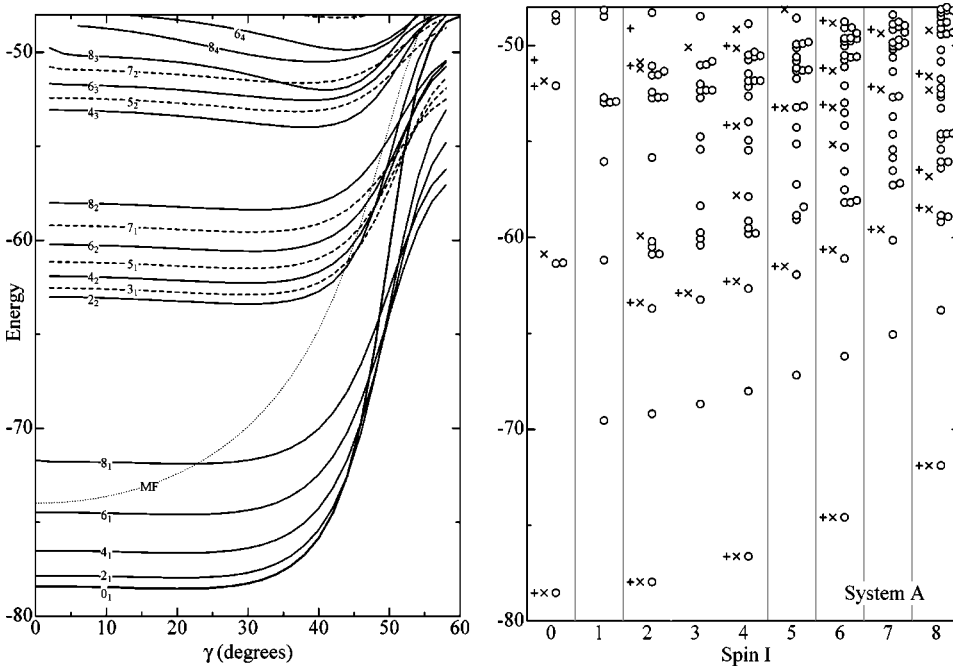


FIG. 2. Energy levels (in MeV) for system A. Left: Functional behavior of PPES's in the deformation limit. The solid (dashed) lines represent PPES's for even (odd) spins. The spin value with a suffix specifying the level ordering is assigned to each PPES. The PES calculated within the mean-field (MF) approximation is indicated by a dotted line. Right: Comparison between the shell model and PGCM levels. The shell model levels are indicated by open circles. The levels of the PGCM1 are specified by + while those of the PGCM2 are specified by \times . See text for further details.

limit. In other words, the intrinsic states with $\gamma=0^\circ-30^\circ$ correspond to a very small range of the full q_0 - q_2 plane.

The triaxiality-favoring tendency of systems *B* and *C* is extended to excited states. The system *B* already exhibits stable triaxial deformation in the stage of the mean-field approximation. In this case, the competition between protons (favoring prolate distribution) and neutrons (favoring oblate distribution) gives rise to stable triaxiality as a whole. At any rate, the triaxial spin projection plays a crucial role in each system from the viewpoint of the correction in energy. Its strong effect drives the equilibrium shape toward large triaxial deformation in the system *C*. The triaxiality-driving effect of the spin projection was our main concern in the

previous works [7–10], but not in the present work. We should keep in mind that such an effect is also seen in the proton-neutron system [12], while we do not go too far into this topic.

Now, we proceed to the analysis of PGCM spectra. The PGCM1 gives an excellent description of the ground-state band and the first quasi- γ band, irrespective of the systems. It can be recognized that the minima of the PPES's also reproduce the levels in the two bands fairly well. For systems *B* and *C*, the projected levels constructed from an intrinsic state with $\gamma=30^\circ$ simulate PGCM levels best of all. Other than these low-lying levels, it is difficult to find clear correspondence between the PGCM1 and the shell model.

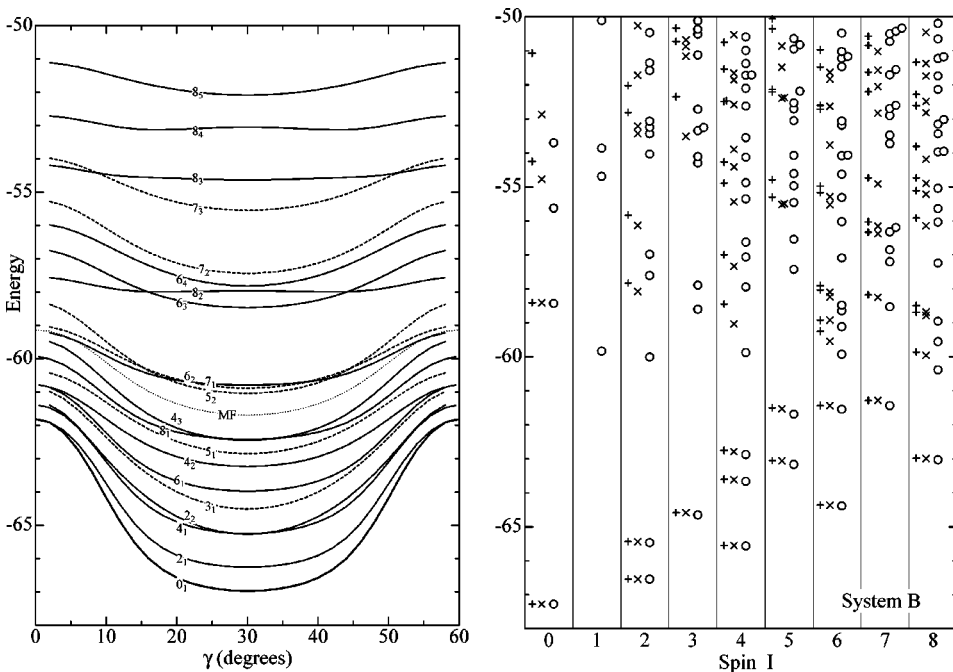


FIG. 3. Energy levels for system *B*. Left: Functional behavior of PPES's in the deformation limit. Right: Comparison between the shell model and PGCM levels. Other illustrations are the same as those in Fig. 2.

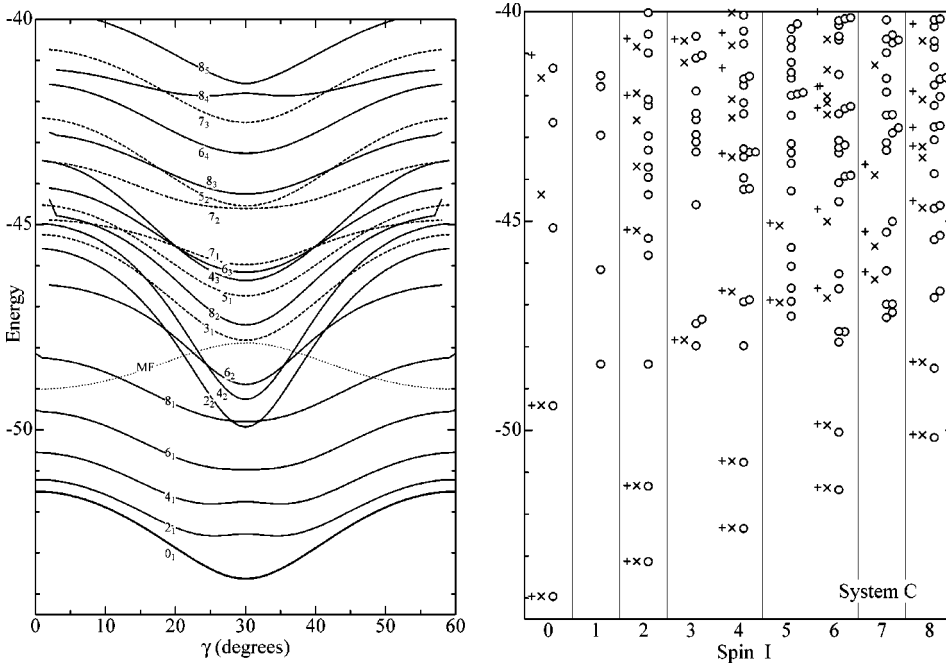


FIG. 4. Energy levels for system C. Left: Functional behavior of PPES's in the deformation limit. Right: Comparison between the shell model and PGCM levels. Other illustrations are the same as those in Fig. 2.

By extending the deformation region in the PGCM2, some new levels appear, and energies of many existing levels are lowered. In the range of higher energy, this extension modifies the results of the PGCM1 to some extent. We find, however, that the addition of states with a small deformation is not essential in the energy range shown in the figures. Further modification is not attained by the increment of deformation points.

In the case of the single- j shell model of protons or neutrons only, the underlying physics is almost clarified in this stage [7–10]. The physical situation is not so simple in the p - n coupled system. There exist many levels even in the low-energy region that cannot be constructed by PGCM1 and PGCM2. A rotational band starting from $I=1_1$ of system A is a typical example. This band is interpreted as the scissors band stemming from the relative displacement of the proton

and neutron distributions [13–15]. The PGCM's in the present section cannot describe such an excitation. In the following section, we intend to simulate various collective modes in a unified manner.

Table I summarizes the number of levels appearing in PGCM1 and PGCM2 for the three systems. Dimensions of the Hamiltonian matrix in the exact shell model and three truncation schemes taken up in the following section are also shown in the table.

There is one thing to be added with respect to the PPES. System B, which is made up of four proton holes and four neutron particles, is very sensitive to the force parameter of the QQI. In Fig. 5, the PPES's for the ground-state band and the first quasi- γ band are displayed. The left panel shows the PPES's for the p - n QQI, and the right panel shows those for the sum of the p - p and n - n components. There is large

TABLE I. The dimension of the Hamiltonian matrix for three model nuclei.

System	PGCM1			PGCM2			One axial state		Axial PGCM		Triaxial PGCM ^a		Exact ^b	
	A	B	C	A	B	C	A,B	C	A,B	C	A,B	C	A,B	C
$I=0$	7	8	7	16	18	15	11	10	168	196	149	141	205	252
$I=1$							10	9	164	187	398	378	509	639
$I=2$	13	17	13	31	35	30	30	27	482	551	680	638	895	1103
$I=3$	6	8	6	13	17	15	28	25	466	527	904	846	1167	1441
$I=4$	18	24	18	40	49	42	46	41	750	845	1148	1062	1501	1821
$I=5$	11	15	11	23	30	24	43	38	714	793	1324	1216	1705	2051
$I=6$	22	30	22	46	57	49	59	52	956	1049	1512	1372	1961	2317
$I=7$	15	21	15	29	38	31	55	48	896	959	1629	1461	2082	2420
$I=8$	25	33	25	49	60	50	69	60	1090	1143	1751	1549	2242	2542
Total	117	156	117	247	304	256	351	310	5686	6250	9495	8663	12267	14586
	Sec. III			Sec. III			Sec. IV A		Sec. IV B		Sec. IV C			

^aNumerical results correspond to one intrinsic state with $\gamma=20^\circ$ for system A, and that with $\gamma=30^\circ$ for systems B and C.

^bThe dimension of which is the same as that of full PGCM truncation.

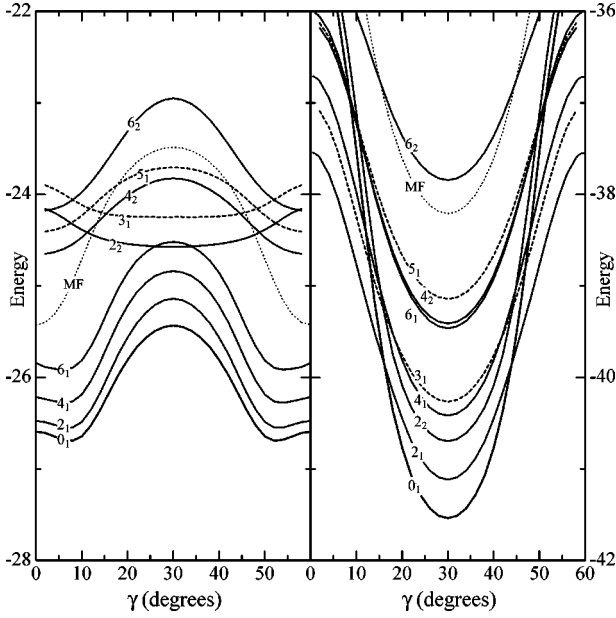


FIG. 5. Functional behavior of PPEs in the deformation limit for system *B*. The PPEs for the ground-state band and the quasi- γ band are displayed up to $I=6$. Left panel shows the contribution from the p - n QQI component (i.e., $\chi_{\pi\pi}=\chi_{\nu\nu}=0$, $\chi_{\pi\nu}=1$), and right panel shows that from the p - p plus n - n QQI component (i.e., $\chi_{\pi\pi}=\chi_{\nu\nu}=1$, $\chi_{\pi\nu}=0$). We use the same convention as those in Figs. 2–4 for the classification of the states.

difference between the two PPEs. The same is true for the unprojected PES. The p - n component has a tendency to cancel the prominent triaxial minimum arising from the p - p and n - n components. However, the stable triaxiality does not disappear from the total PPE until the ratio $\chi_{\pi\nu}/\chi_{\pi\pi}$ ($\chi_{\pi\nu}/\chi_{\nu\nu}$) becomes extremely large. Such a characteristic effect appears when two kinds of nucleons are definitely separated into the prolate and oblate distributions. For systems *A* and *C*, functional behavior of the PPEs against γ is not affected by the force parameter. Systems *B* and *C* possess some common features, including electromagnetic transition properties, but their χ dependence is quite different.

It is still controversial whether such an ambiguity for the QQI is also seen in real nuclei. It is known that the long-range particle-hole $T=0$ component of the p - n QQI is crucial for the nuclear deformation. The requirement of the identical proton and neutron mean fields makes the p - n component dominant, in general. In many transitional nuclei or weakly deformed γ -soft nuclei, a combination of valence particles and valence holes determines fundamental nuclear properties. It will be interesting to investigate a role of the p - n interaction in connection with the triaxiality.

IV. PGCM TRUNCATION OF THE SHELL MODEL

Within the PGCM examined in the preceding section, total spin I is projected out directly from the p - n product wave function $|\Phi\rangle=|\Phi_\pi\rangle|\Phi_\nu\rangle$. In such a construction of the PGCM state, the proton and neutron bodies are tightly coupled, and both states of $|\Phi_\pi\rangle$ and $|\Phi_\nu\rangle$ undergo the same rotation specified by the common set of Euler angles. Its

theoretical framework cannot treat various collective modes in which the relative motion of protons and neutrons is essential. The extension of the framework is necessary to describe such modes.

One possibility is to exclude the assumption of common deformation between protons and neutrons. Each shape degree of freedom \mathbf{q}_τ ($\tau=\pi, \nu$) is regarded as two independent generator coordinates, but total spin is still projected out from the p - n product wave function. This scheme can partially take into account the p - n relative motion. At any rate, many levels in odd K bands cannot be described as long as the PGCM is based on intrinsic states conserving the D_2 symmetry.

An alternative method is to project out spins of the proton and neutron parts (I_π and I_ν) separately, and to construct the total wave function from the angular momentum coupling. Then, the proton and neutron PGCM wave functions are provided independently, and the Hill-Wheeler equation is solved twice. The PGCM wave function for each nucleon system is given by

$$|\Psi_{I_\rho M_\tau N_\tau}^{(\tau)}\rangle = \int d\mathbf{q}_\tau \sum_{K_\tau=-I_\tau}^{I_\tau} \mathcal{F}_{K_\tau \rho}^{I_\tau N_\tau}(\mathbf{q}_\tau) \hat{P}_{M_\tau K_\tau}^{I_\tau} \hat{P}^{N_\tau} |\Phi_\tau(\mathbf{q}_\tau)\rangle, \quad (8)$$

where $N_\nu=N$, $N_\pi=Z$, and \mathbf{q}_τ integral is carried out over the range relevant to protons or neutrons. The weight functions $\mathcal{F}_{K_\tau \rho}^{I_\tau N_\tau}(\mathbf{q}_\tau)$ are solutions of the Hill-Wheeler equation

$$\int d\mathbf{q}'_\tau \sum_{K'_\tau=-I_\tau}^{I_\tau} \{ \langle \Phi_\tau(\mathbf{q}_\tau) | \hat{H}_\tau \hat{P}_{K'_\tau K_\tau}^{I_\tau} \hat{P}^{N_\tau} | \Phi_\tau(\mathbf{q}'_\tau) \rangle - E_{I_\tau \rho} \langle \Phi_\tau(\mathbf{q}_\tau) | \hat{P}_{K'_\tau K_\tau}^{I_\tau} \hat{P}^{N_\tau} | \Phi_\tau(\mathbf{q}'_\tau) \rangle \} \mathcal{F}_{K'_\tau \rho}^{I_\tau N_\tau}(\mathbf{q}'_\tau) = 0. \quad (9)$$

An essential point of this scheme is the separation of I_π and I_ν rather than the discrimination between proton and neutron deformations. As mentioned in Sec. II, we utilize deformation points \mathbf{q}_π and \mathbf{q}_ν determined from common parameters (β , γ). Up to Eq. (9), unlike nucleons are completely separated.

In the practice of the numerical analysis, we project out all the possible spin values for I_π and I_ν to make up the total spin I . The range of I_π , I_ν runs from $I_\pi=I_\nu=0$ to $\max(I_\pi)=\max(I_\nu)=20$ for systems *A* and *B*, and $\max(I_\pi)=\max(I_\nu)=18$ for system *C*. We also take account of the K_τ quantum number correctly in order to count the dimension of the Hamiltonian matrix without ambiguity. Needless to say, high spins I_τ and high K_τ components as well as high-lying states specified by large ρ are not important for low-lying collective levels. In case of realistic nuclei, the contribution from these will be safely excluded without affecting key dynamics.

The p - n coupled state is constructed from the proton and neutron PGCM wave functions

$$|\Psi_{IMNZ}(I_\pi \rho, I_\nu \sigma)\rangle = [|\Psi_{I_\pi \rho Z}^{(\pi)}\rangle |\Psi_{I_\nu \sigma N}^{(\nu)}\rangle]_M^I. \quad (10)$$

What we intend in the following investigation is to construct the p - n coupled state in terms of various kinds of PGCM's. The p - n coupled PGCM states provide building blocks for the truncation of the shell model. The truncated shell model wave function for the k th state of spin I is given by

$$|\psi_{I\kappa MNZ}\rangle = \sum_{I_\pi\rho} \sum_{I_\nu\sigma} f_{I\kappa}(I_\pi\rho, I_\nu\sigma) |\Psi_{IMNZ}(I_\pi\rho, I_\nu\sigma)\rangle. \quad (11)$$

The p - n correlation arising from the $\hat{H}_{\pi\nu}$ term does not appear until the total Hamiltonian matrix is diagonalized in the $(I_\pi\rho, I_\nu\sigma)$ space.

Here, we give the Hamiltonian matrix element concerning the p - n coupled PGCM wave function of Eq. (10). The matrix for identical nucleons is diagonal, and its elements are just the PGCM energies given by the Hill-Wheeler equation

$$\begin{aligned} &\langle \Psi_{IMNZ}(I_\pi\rho, I_\nu\sigma) | (\hat{H}_\pi + \hat{H}_\nu) | \Psi_{IMNZ}(I'_\pi\rho', I'_\nu\sigma') \rangle \\ &= (E_{I_\pi\rho} + E_{I_\nu\sigma}) \delta_{I_\pi, I'_\pi} \delta_{I_\nu, I'_\nu} \delta_{\rho, \rho'} \delta_{\sigma, \sigma'}. \end{aligned} \quad (12)$$

The matrix element of the p - n interaction is

$$\begin{aligned} &\langle \Psi_{IMNZ}(I_\pi\rho, I_\nu\sigma) | \hat{H}_{\pi\nu} | \Psi_{IMNZ}(I'_\pi\rho', I'_\nu\sigma') \rangle \\ &= -\chi_{\pi\nu} \mathcal{W}(I'_\pi 2I_\nu; I_\pi I'_\nu) \times \langle \Psi_{I_\pi\rho Z}^{(\pi)} | \hat{Q}^{(\pi)} | \Psi_{I'_\pi\rho' Z}^{(\pi)} \rangle \\ &\quad \times \langle \Psi_{I_\nu\sigma N}^{(\nu)} | \hat{Q}^{(\nu)} | \Psi_{I'_\nu\sigma' N}^{(\nu)} \rangle, \end{aligned} \quad (13)$$

with the reduced matrix element

$$\begin{aligned} &\langle \Psi_{I_\pi\rho N}^{(\pi)} | \hat{Q}^{(\pi)} | \Psi_{I'_\pi\rho' N}^{(\pi)} \rangle \\ &= \sqrt{2I_\pi+1} \int d\mathbf{q}_\tau \int d\mathbf{q}'_\tau \sum_{K_\tau=-I_\tau}^{I_\tau} \sum_{K'_\tau=-I'_\tau}^{I'_\tau} \sum_{\mu=-2}^2 \\ &\quad \times (I'_\tau K_\tau - \mu, 2\mu | I_\tau K_\tau) \\ &\quad \times \langle \Phi_\tau(\mathbf{q}_\tau) | \hat{Q}_\mu^{(\pi)} \hat{P}_{K_\tau - \mu K'_\tau}^{I_\tau} \hat{P}^{N_\tau} | \Phi_\tau(\mathbf{q}'_\tau) \rangle \\ &\quad \times \mathcal{F}_{K_\tau\rho}^{I_\tau N_\tau*}(\mathbf{q}_\tau) \mathcal{F}_{K'_\tau\rho'}^{I'_\tau N_\tau}(\mathbf{q}'_\tau), \end{aligned} \quad (14)$$

where $(j_1 m_1, j_2 m_2 | j_3 m_3)$ and \mathcal{W} denote the Clebsch-Gordan coefficient and the Racah coefficient, respectively. Throughout this paper, the definition of the reduced matrix element for the irreducible spherical tensor of rank λ and label μ , $\hat{T}_{\lambda\mu}$, is

$$\langle IM\alpha | \hat{T}_{\lambda\mu} | I'M'\alpha' \rangle = \frac{(I'M', \lambda\mu | IM)}{\sqrt{2I+1}} \langle I\alpha | \hat{T}_\lambda | I'\alpha' \rangle. \quad (15)$$

A. PGCM with only one axial intrinsic state

In the first place, we consider the case of one axial intrinsic state ($\gamma=0^\circ$) in the deformation limit. The PGCM state is obtained by replacing the weight function in Eq. (8) according to

$$\mathcal{F}_{K_\tau\rho}^{I_\tau N_\tau}(\mathbf{q}_\tau) \rightarrow \frac{\delta_{K_\tau 0} \delta(q_{0\tau} - \max[q_{0\tau}]) \delta(q_{2\tau} - 0)}{\langle \Phi_\tau(\gamma=0^\circ) | \hat{P}_{00}^{I_\tau} | \Phi_\tau(\gamma=0^\circ) \rangle}. \quad (16)$$

This theoretical framework is essentially equivalent to that of the extended version of the projected shell model [16]. The spin I_τ has to be even, and only one state is allowed for each spin. Then, the summation for the level indices ρ and σ in Eq. (11) can be dropped. The restriction to a prolate shape in the deformation limit allows us to omit the particle-number projection, and to replace the triaxial spin projection with the axial one. Thus, the PGCM state becomes simple enough, but physical contents derived from it are still rich. In order to demonstrate this, we take a close look at the degenerate $2p1f$ shell before the single- j shell.

It was shown that the SD -pair truncation of the shell model exactly reproduces dominant irreps for the $2s1d$ shell [17]. The $2p1f$ shell, for which the SD -pair approximation is obviously insufficient, is suitable for checking the validity of the simplification. Let us consider a system with six protons and six neutrons as an example.

Our Hamiltonian consists of pure QQI with $\chi = \chi_{\pi\pi} = \chi_{\nu\nu} = \chi_{\pi\nu}$ (symmetric between protons and neutrons). As a result, Elliott's $SU(3)$ model can be applied to this situation [18,19]. The p - n coupled system has the dynamical symmetry $SU(3)_{\pi} \otimes SU(3)_{\nu} \supset SU(3)_{\pi\nu}$. The leading representation is $(\lambda, \mu)_{\tau} = (12, 0)_{\tau}$ ($\tau = \pi, \nu$) for identical nucleons. This representation has the maximum orbital symmetry, i.e., zero intrinsic spin $S_{\pi} = S_{\nu} = 0$, so that I_{π}, I_{ν} , and the total spin I are identical with the orbital angular momenta L_{π}, L_{ν} , and L , respectively. The energy spectra of the total system are given by using the eigenvalue of the second order $SU(3)_{\pi\nu}$ Casimir operator

$$\begin{aligned} E_L(\lambda, \mu)_{\pi\nu} &= -\frac{5\chi}{32\pi} [4(\lambda^2 + \lambda\mu + \mu^2 + 3\lambda + 3\mu) \\ &\quad - 3L(L+1)]. \end{aligned} \quad (17)$$

If the spin projection is applied to the prolate Nilsson state with six like nucleons in the degenerate $2p1f$ shell, the $SU(3)_{\tau}$ representation $(12, 0)_{\tau}$ is exactly reproduced. Then, unlike nucleons are coupled through the diagonalization of the total Hamiltonian. This procedure generates rotational bands belonging to the $SU(3)_{\pi\nu}$ irreps, $(12, 0)_{\pi} \otimes (12, 0)_{\nu} = (24, 0)_{\pi\nu} \oplus (22, 1)_{\pi\nu} \oplus \dots \oplus (0, 12)_{\pi\nu}$. A total of 413 levels belonging to the above irreps are exactly reproduced within the PGCM truncation. In Fig. 6, the energy spectra are displayed. We point out without details that only one representation $(24, 0)_{\pi\nu}$, i.e., the ground-state band, is reproduced when the spin projection is applied directly to the total Nilsson state as in the preceding section. The excited bands arise from the relative motion between protons and neutrons, since

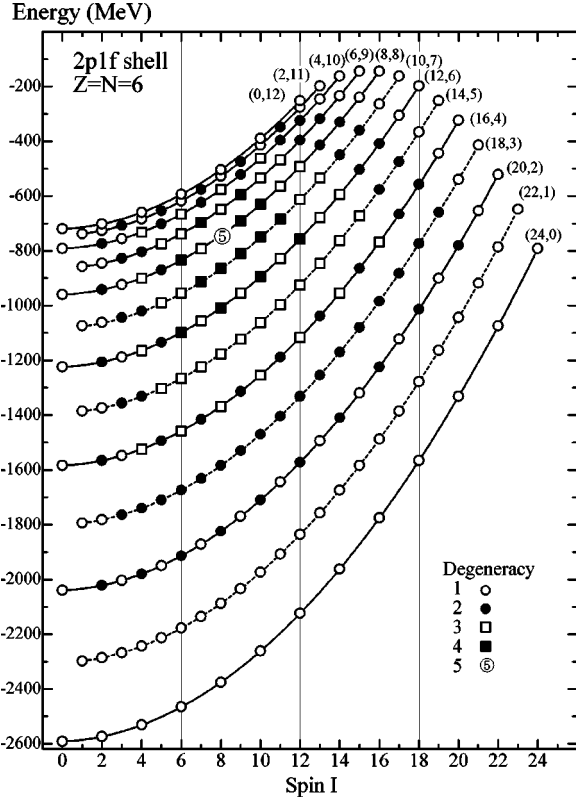


FIG. 6. Energy levels for the degenerate $2p1f$ shell. For the sake of convenience, the force parameter of the QQI is chosen to be $\chi = 32\pi/5$ MeV. Each rotational band is specified by the $SU(3)_{\pi\nu}$ irreps, $(\lambda, \mu)_{\pi\nu}$. With respect to Elliott's K number, even (odd) K bands are connected by solid (dashed) lines.

both intrinsic states are in the irreps $(12,0)_{\pi}$ and $(12,0)_{\nu}$, corresponding to their ground state [16]. The first excited band starting from $I_{\kappa}=1_1$, namely, the $K=1$ band¹ described by the representation $(22,1)_{\pi\nu}$, is interpreted as the rotational band on the scissors vibrational mode.

We now leave the multi- j shell and apply the same method to system A. The low-lying rotational bands are shown in Fig. 7. These consist of the lowest 25 levels calculated in the PGCM subspace and the corresponding exact levels. There appear 51 shell model levels in the energy range of the lowest 25 approximate levels. It can be recognized that the band structure is similar to that of the degenerate $2p1f$ shell. In addition to the ground-state band, two bands interpreted as the first quasi- γ band and β band are reproduced qualitatively. The $I_{\kappa}=1_1$ band, which cannot be simulated by the PGCM in Sec. III, is also reproduced with a good accuracy. In spite of its drastic simplification, many correlations are already taken into account. The total number of levels up to $I=8$ amounts to 351.

However, we must regard the success for system A as an exceptional case. The picture of the $SU(3)$ model happens to be suitable for this system owing to some conditions, e.g.,

¹The assignment of K is based on Elliott's quantum number. Within the present PGCM state generated from any axial intrinsic state, the K number is necessarily zero.

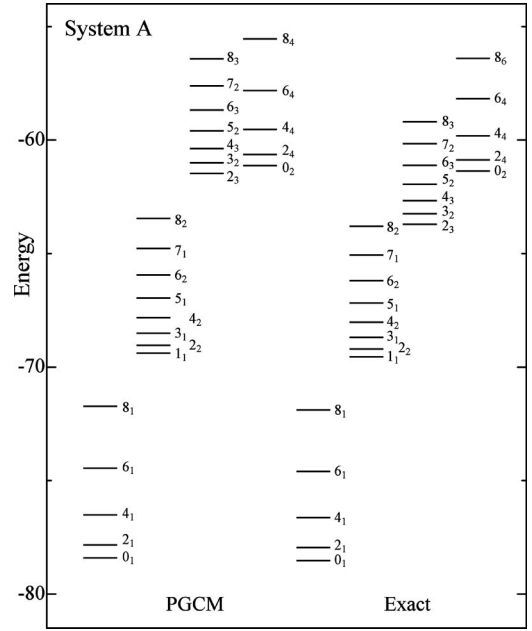


FIG. 7. Energy levels in the exact shell model and the PGCM subspace with one prolate intrinsic state for system A. From the left, the ground-state band, the scissors band, the quasi- γ band, and the β band are depicted for both theoretical methods. See text for further details.

the shell fillings and model Hamiltonian. Turning our attention to systems B and C , we see that the problem is not so simple. The correspondence between the PGCM truncation and the exact shell model is bad, though their figures are not displayed here. There is large discrepancy even in the ground-state energy. As we have seen in Figs. 3 and 4, two projected levels at prolate and oblate shapes are degenerate in energy, and the minimum of the PPES appears at $\gamma = 30^\circ$. It is obvious that one intrinsic state with $\gamma=0^\circ$ is insufficient to simulate the complicated band structure of systems B and C . Now that underlying physics for system A has been clarified, we place great emphasis on the analysis of the systems B and C in what follows.

B. Axial PGCM

One of the purposes of this paper is to investigate various kinds of PGCM's by changing the choice of generator coordinates. We cannot evade examining the capability of the axial PGCM, since its application is interesting from a practical viewpoint. The restriction to axial shapes is still effective to cut down the computation time, while the configuration mixing of many deformation points is required. In this section, we focus on the truncation of the shell model in terms of the axial PGCM.

The wave function of the axial PGCM is obtained by setting $q_{2\tau}=0$ ($\gamma=0^\circ$) and $K_{\tau}=0$ in Eq. (8),

$$|\Psi_{I_{\rho M} \tau N_{\tau}}^{(\tau)}\rangle = \int dq_{0\tau} \mathcal{F}_{0\rho}^{I_{\rho} N_{\tau}}(q_{0\tau}) \hat{P}_{M_{\rho} 0}^{I_{\rho}} \hat{P}_{\tau}^{N_{\tau}} |\Phi_{\tau}(q_{0\tau})\rangle, \quad (18)$$

where $q_{0\tau}$ is integrated over all the possible axially symmet-

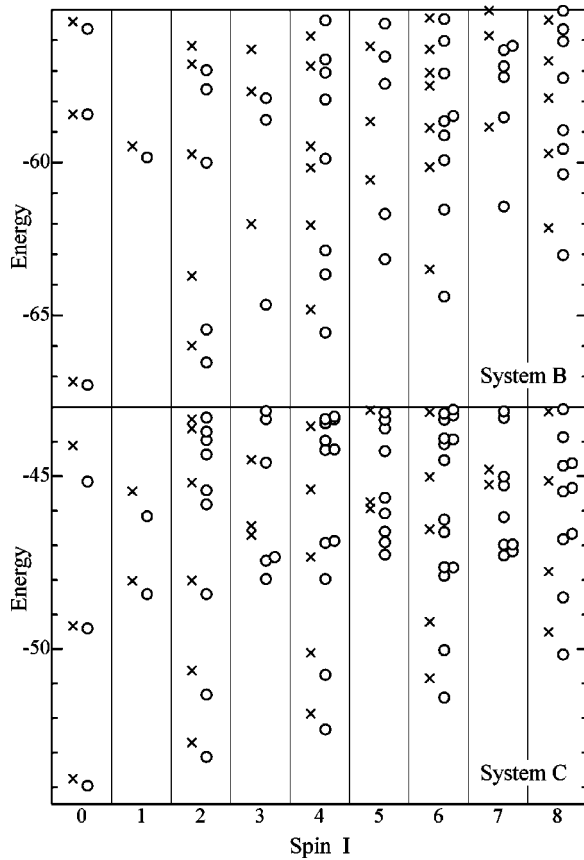


FIG. 8. Energy levels in the exact shell model and the axial PGCM subspace for systems *B* and *C*. The shell model levels are indicated by open circles, and the levels of the PGCM truncation by crosses.

ric shapes. We take about 50 deformation points uniformly over the whole range of $q_{0\tau}$. For all the systems, the number of levels already reaches the maximum within its theoretical framework (cf. Table I), and the convergence of each level is confirmed.

For system *A*, we only point out a few facts without showing the figure. In comparison with the result in the previous section (Fig. 7), the agreement between the levels calculated in the axial PGCM subspace and the exact ones becomes even better, but no drastic change is made in the low-lying levels. This validates an assumption of a fixed intrinsic state.

The numerical results for systems *B* and *C* are shown in the upper and lower panels of Fig. 8, respectively. The level schemes calculated in the PGCM subspace are compared with the exact ones. The truncation by the axial PGCM is not very good as a whole. The axial intrinsic state includes only even spin components so that the odd spin I_τ does not appear in the axial PGCM. All the even and odd spins of the p - n coupled PGCM state are constructed by the angular momentum coupling of even I_π and I_ν . The absence of the odd spin I_τ is a main reason for the discrepancy between the PGCM truncation and the exact shell model. This view is eventually reduced to the absence of the triaxial intrinsic state.

However, the accuracy of lower-spin states is satisfactory. Above all, the states of $I=0$, for which $I_\pi=I_\nu$, are well reproduced. This is because shell model states of odd I_π (I_ν)

are not dominant in the low-energy range for the proton (neutron) system. Moreover, the accuracy of the ground-state band is not so bad. It is worthwhile to mention that bad results in the case of one prolate intrinsic state are improved substantially. What must be stressed is that the axial PGCM has an ability to reproduce many states of even spin I_τ , including the members of quasi- γ bands, while K_τ is restricted to zero [8]. Many of these levels are usually classified into states in the $K_\tau \neq 0$ bands in other theories. Thus, capabilities hidden in each identical nucleon system lead to the improvement of spectra.

It can be safely said that the truncation by the axial PGCM will be a good and practical approximation for many deformed nuclei. Also, it may be conveniently utilized as the first approximation even for the triaxial or γ -soft nucleus.

C. Triaxial PGCM

The consequence of the preceding section requires us to withdraw the assumption of the axially symmetric deformation for further progress. Let us consider the PGCM state generated from a triaxial intrinsic state in the deformation limit

$$|\Psi_{I_\tau M_\tau N_\tau}^{(\tau)}\rangle = \sum_{K_\tau=-I_\tau}^{I_\tau} \mathcal{F}_{K_\tau}^{I_\tau N_\tau}(\gamma) \hat{P}_{M_\tau K_\tau}^{I_\tau} |\Phi_\tau(\gamma)\rangle. \quad (19)$$

Other than the triaxiality, there is no large difference between the triaxial PGCM state and that in Sec. IV A.

In Fig. 9, the lowest 300 shell model levels and the corresponding levels calculated in the PGCM subspace are displayed for systems *B* and *C*. The numerical analysis is performed by using an intrinsic state with $\gamma=30^\circ$ for both systems. The number of levels increases drastically due to the triaxial degree of freedom, though the configuration mixing of deformation points is not carried out. There appear 274 (235) levels in the figure for system *B* (*C*).

The strong influence of the triaxial intrinsic state can be also read from the dimension of the Hamiltonian matrix shown in Table I. In comparison with the axial PGCM truncation, the dimension increases except for the state of $I=0$. The axial PGCM truncation can produce at most half of the total levels. This implies that many additional levels originate from the triaxiality. In addition to the scissors mode, the triaxiality of the proton and neutron distributions excites new modes such as the twist mode, scissors plus twist mode, and so forth [20]. These modes are also visualized as a counter-rotational oscillation of the triaxial proton and neutron bodies.

There is still room to make an improvement, but the overall trend of exact spectra is well simulated. Considering the fact that the result is obtained by using an only intrinsic state with $\gamma=30^\circ$, we may say that the triaxial PGCM is very successful.

For system *A*, we abbreviate the figure, and only refer to some outcomes. The result is almost perfect. The truncation is already successful in the stage of the axial PGCM, but further modification is achieved. For instance, the band head energy of the first quasi- γ band, which is not quantitatively

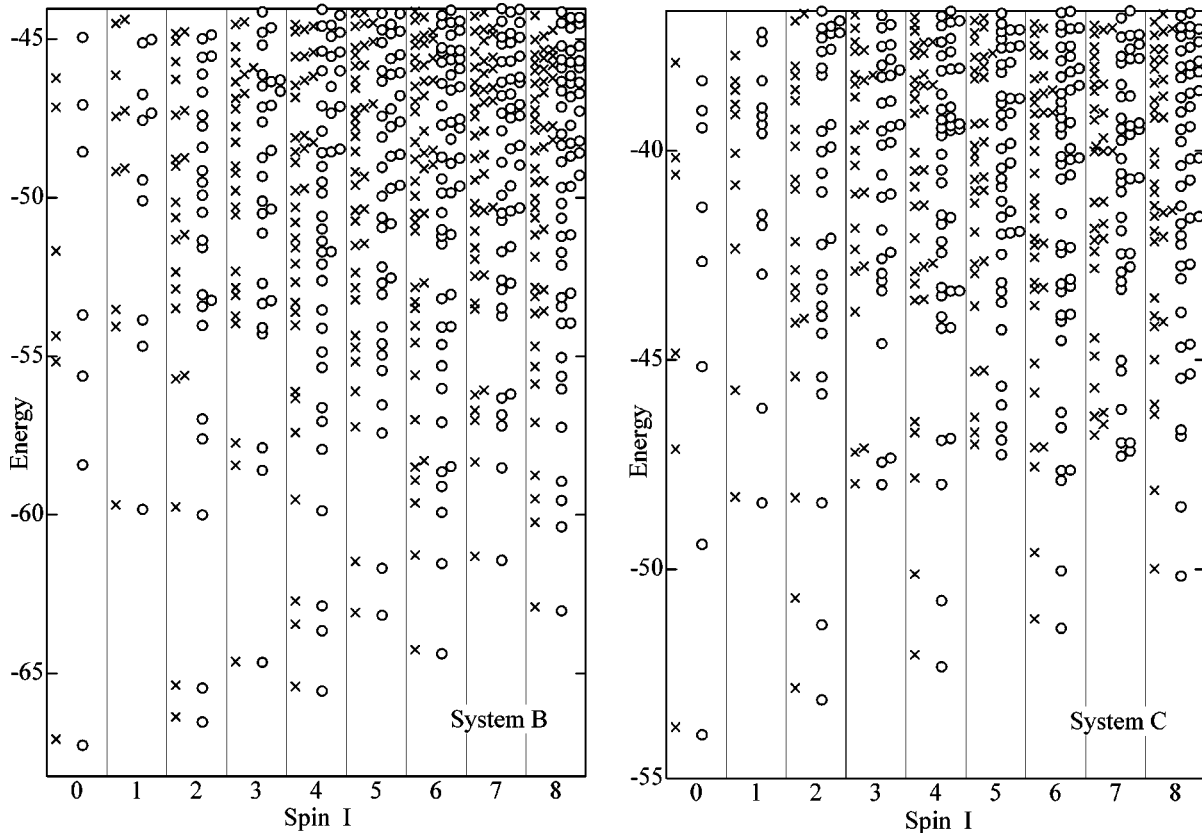


FIG. 9. Energy levels in the exact shell model and the $\gamma=30^\circ$ triaxial PGCM subspace for systems *B* (left) and *C* (right). The shell model levels are indicated by open circles, and the levels of the PGCM truncation by crosses. The lowest 300 shell model levels are displayed.

reproduced by the axial PGCM, is improved with the help of triaxiality. The number of levels amounts to 282 in the energy range of the lowest 300 shell model levels, when an intrinsic state with $\gamma=20^\circ$ is employed.

Indeed the truncation is successful, but the underlying physics derived from it is not so clear. It is not always significant to extend the theoretical framework at the cost of an intuitive physical picture that simpler schemes have. In the PGCM, such a picture is provided by intrinsic states. As in the preceding section, we can depict the PPES in the space of deformation parameters.

In Fig. 10, the PPES's of the systems *B* and *C* are displayed as functions of γ . Because of a large number of levels, we confine our investigation to low-lying states of $I=0, 1$, and 2. Some levels are not smooth around the axially symmetric shape ($\gamma\sim 0^\circ$ or 60°). Through this range, the dimension of the Hamiltonian matrix increases rapidly, and new levels appear. The levels constructed at $\gamma=30^\circ$ give the best description of exact levels. This result is easily understood from the above investigations. It is noted that the triaxiality-favoring tendency is extended to the states of $I=1$. The scissors $I_\kappa=1_1$ state and the ground state possess common properties with respect to the triaxiality. In the following section, we will examine this issue, in connection with the $M1$ and $E2$ transition probabilities.

It is interesting to compare the PPES's in this section with those in Sec. III. Over the whole range of γ , the energy of each level is lower than those of Figs. 3 and 4, while the

appearance of the PPES's is preserved as a whole. Their variation against γ turns out to be small, in general. In other words, the minima of the PPES's become shallow compared with Figs. 3 and 4. (One clear example for this feature is seen in system *A*, where the ground-state energy at $\gamma\sim 60^\circ$ is lowered by almost 20 MeV, in comparison with the PPES in Fig. 2.) This fact implies that a large correlation is taken into account through the p - n coupling scheme, even if a selected intrinsic state is not the most suitable. On the other hand, some levels, e.g., the state of $I_\kappa=0_2$, become less accurate than the axial PGCM case. The restriction to a fixed shape is not appropriate to reproduce these levels quantitatively.

As inferred from the above excellent results, the configuration mixing of some triaxial intrinsic states completes the work at least for the p - n single- j shell model. As a matter of fact, the "full" PGCM in Eq. (8) makes a perfect reproduction of all the shell model levels for the three systems. Total number of levels up to $I=8$ already amounts to 10 000. This fact indicates that the single- j shell model for the identical nucleon system is exactly solved in terms of the PGCM. The purpose of this paper is not to bring the PGCM truncation to perfection. It goes without saying that this kind of endeavor makes no sense from a practical point of view. Therefore, we do not take up the "full" PGCM in detail.

The excellence of the PGCM may conversely suggest the difficulty in the numerical calculation. Namely, as is always the case with the spherical shell model, the PGCM truncation may be confronted with the diagonalization of the Hamil-

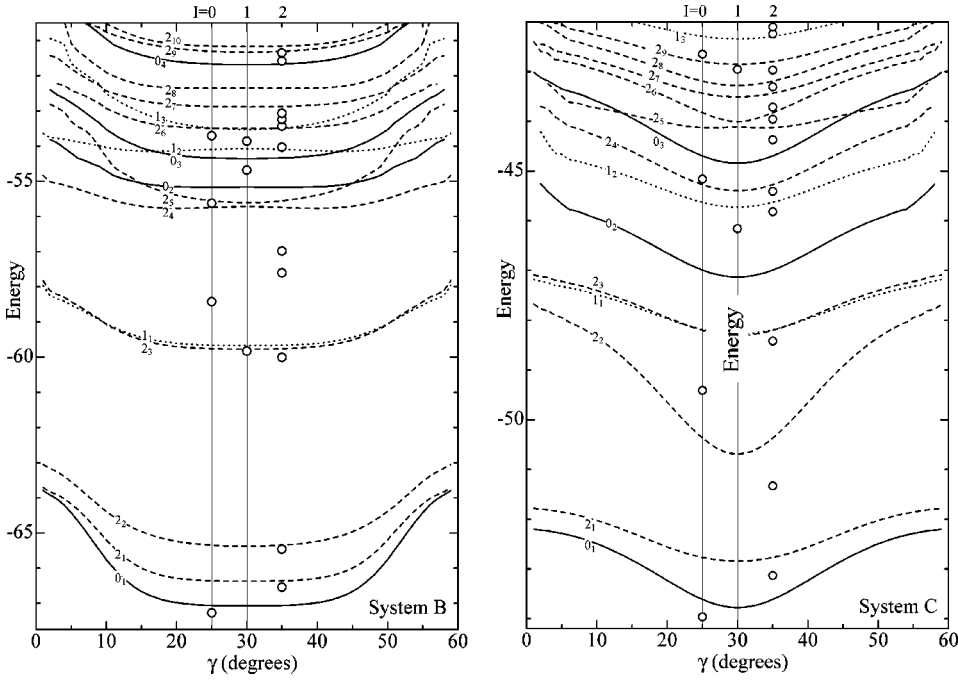


FIG. 10. Functional behavior of PPEs's calculated in the triaxial PGCM subspace for systems *B* (left) and *C* (right). The lowest PPEs's for $I=0$ (solid lines), 1 (dotted lines), and 2 (dashed lines) are displayed. For comparison, exact shell model levels of $I=0$, 1, and 2 (open circles) are plotted in the lines of $\gamma=25^\circ$, 30° , and 35° , respectively. See text for further details.

tonian matrix with huge dimension, if it is faithfully applied to the analysis of a real heavy nucleus. It is natural to ask whether the “full” PGCM truncation is still applicable to realistic cases. The present model nuclei are not suitable for answering this question, since the full PGCM truncation is no longer an approximation within the p - n single- j shell model. The perfect reproduction is simply due to the smallness and simplicity of the system. It is impossible to connect the result of the p - n single- j shell directly to realistic nuclei. However, we can give some comments on this issue.

The dimension of the Hamiltonian matrix can be kept small as long as the number of deformation points is small. Inclusion of a few triaxial intrinsic states has a large effect on the PGCM wave function. The minimum number of points to attain the perfect reproduction of the shell model is only two for systems *A* and *B*, and three for system *C*. What must not be forgotten is that the PGCM2 examined in Sec. III takes account of as many as 30 points, the results of which are inferior to the present ones. In any case, a small number of deformation points is sufficient to reproduce low-lying collective levels. We consider that this view is correct even in real nuclei. In addition to some implicit assumptions in the intrinsic state, imposing a restriction on deformation points works to suppress the dimension of the Hamiltonian matrix. Some simplifications of the PGCM state may be inevitable, but the knowledge of intrinsic states and PPEs's is expected to offer a useful ansatz for the truncation.

V. ELECTROMAGNETIC PROPERTIES

It is interesting to examine electromagnetic (EM) properties as an application of the PGCM. Such a study also gives a chance to test the validity of the wave function. In this section, we employ the p - n coupled state constructed from two PGCM wave functions of Eqs. (18) and (19), and analyze $B(M1/E2)$ values for the systems *B* and *C*. In parallel

with this, we pay attention to their γ dependence.

Here, we give some expressions for the sake of completeness. We start from the irreducible tensor operator $\hat{T}_{\lambda\mu}$ of rank λ and label μ ,

$$\hat{T}_{\lambda\mu} = \hat{T}_{\lambda\mu}^{(\pi)} + \hat{T}_{\lambda\mu}^{(\nu)}. \quad (20)$$

By using the truncated shell model wave function of Eq. (11), a reduced EM multipole transition probability is given by

$$B(E\lambda/M\lambda; I_i\kappa_i \rightarrow I_f\kappa_f) = \frac{1}{2I_i+1} |\langle \psi_{I_f\kappa_f NZ} \| \hat{T}_\lambda \| \psi_{I_i\kappa_i NZ} \rangle|^2 \quad (21)$$

with

$$\begin{aligned} & \langle \psi_{I_f\kappa_f NZ} \| \hat{T}_\lambda \| \psi_{I_i\kappa_i NZ} \rangle \\ &= \sqrt{(2I_i+1)(2I_f+1)} \sum_{I_\pi\rho} \sum_{I_\nu\sigma} \sum_{I'_\pi\rho'} \sum_{I'_\nu\sigma'} \\ & \times [(-1)^{I_f+I'_\pi-I_\nu-\lambda} \delta_{I_\nu, I'_\nu} \delta_{\sigma, \sigma'} \\ & \times \langle \Psi_{I_\pi\rho Z}^{(\pi)} \| \hat{T}_\lambda^{(\pi)} \| \Psi_{I'_\pi\rho' Z}^{(\pi)} \rangle \mathcal{W}(I_\pi I'_\pi I_f I_i; \lambda I_\nu) \\ & + (-1)^{I_i+I_\nu-I_\pi-\lambda} \delta_{I_\pi, I'_\pi} \delta_{\rho, \rho'} \\ & \times \langle \Psi_{I_\nu\sigma N}^{(\nu)} \| \hat{T}_\lambda^{(\nu)} \| \Psi_{I'_\nu\sigma' N}^{(\nu)} \rangle \mathcal{W}(I_\nu I'_\nu I_f I_i; \lambda I_\pi)] \\ & \times f_{I_f\kappa_f}^* (I_\pi\rho, I_\nu\sigma) f_{I_i\kappa_i} (I'_\pi\rho', I'_\nu\sigma'). \end{aligned} \quad (22)$$

In the single- j shell model, both the orbital angular momentum $\hat{\mathbf{L}}$ and the intrinsic spin $\hat{\mathbf{S}}$ are identical with the total spin $\hat{\mathbf{J}}$ multiplied by a trivial factor so that the $M1$ operator is given by

$$\hat{T}(M1; \mu) = \sqrt{\frac{3}{4\pi}} \sum_{\tau=\pi, \nu} \left(g_l^\tau + \frac{g_s^\tau - g_l^\tau}{2j} \right) \hat{J}_\mu^{(\tau)}, \quad (23)$$

where we employ the choice $j = l + 1/2$ throughout this paper. In the numerical analysis, we use the *bare* orbital and spin gyromagnetic factors, i.e., $g_l^\pi = 1$, $g_s^\pi = 5.5857$ for protons and $g_l^\nu = 0$, $g_s^\nu = -3.8263$ for neutrons. The dynamical effect on the $M1$ strength arises only from the coefficient $f_{I_\kappa}(I_\pi \rho, I_\nu \sigma)$ of the shell model wave function, since the reduced matrix element does not connect different PGCM states, giving a geometrical contribution only,

$$\langle \Psi_{I_\pi \rho N_\tau}^{(\tau)} \| \hat{J}_\mu^{(\tau)} \| \Psi_{I_\nu \rho' N_\tau}^{(\tau)} \rangle = \delta_{I_\tau, I_\tau'} \delta_{\rho, \rho'} \sqrt{I_\tau(I_\tau + 1)(2I_\tau + 1)}. \quad (24)$$

The $E2$ operator is defined as

$$\hat{T}(E2; \mu) = e_\pi \hat{Q}_\mu^{(\pi)} + e_\nu \hat{Q}_\mu^{(\nu)}, \quad (25)$$

where e_π and e_ν indicate the effective charges of protons and neutrons, respectively. The general form of the reduced matrix element is already given in Eq. (14). In the practice of the numerical analysis, we utilize the effective charges $(e_\pi, e_\nu) = (1.5, 0.5)$ as an example. For the present model nucleus, the $B(M1/E2)$ value is given as a dimensionless quantity.

We put our emphasis mainly on the EM transitions, which have a connection with the $I_\kappa = 1_1$ state excited through the scissors mode. For the systems of the p - n single- j shell, the $M1$ transition from the ground state to the lowest $I_\kappa = 1_1$ scissors state exhausts almost the total $M1$ strength

$$\frac{B(M1; 0_1 \rightarrow 1_1)}{\sum_{\kappa=1}^{\text{all}} B(M1; 0_1 \rightarrow 1_\kappa)} > 0.95. \quad (26)$$

Clear fragmentation of the $M1$ strength, which is typical of realistic nuclei, does not occur in the p - n single- j shell model within the present framework.

Table II summarizes some $B(M1/E2)$ values relevant to the $I_\kappa = 1_1$ scissors state for systems B and C . We also present other transitions in order to understand the interrelation between the scissors and neighboring states. The exact $B(M1/E2)$ values are compared with the results of two kinds of PGCM truncations; one is the axial PGCM in Sec. IV B and the other is the triaxial PGCM in Sec. IV C. For the triaxial PGCM, we employ an intrinsic state with $\gamma = 30^\circ$ in view of the triaxiality-favoring tendency of the PPES.

It can be said that both truncation schemes reproduce general trends of the exact results very well. In Sec. IV B, we have pointed out the potentiality of the axial PGCM even for

TABLE II. Comparison of exact $B(M1/E2)$ values with the results of the PGCM truncations for systems B and C .

		Exact	$\gamma = 30^\circ$	Axial
System B	$B(M1; 1_1 \rightarrow 0_1)$	0.6565	0.6496	0.6754
	$B(M1; 1_1 \rightarrow 2_1)$	0	0	0
	$B(M1; 1_1 \rightarrow 2_2)$	1.3104	1.3309	1.3294
	$B(M1; 1_1 \rightarrow 2_3)$	0.0946	0.1122	0.0753
	$B(E2; 1_1 \rightarrow 2_1)$	0.6862	0.6697	0.7032
	$B(E2; 1_1 \rightarrow 2_2)$	0.1032	0.1063	0.3473
	$B(E2; 1_1 \rightarrow 2_3)$	64.6279	71.1025	60.2517
	$B(E2; 2_1 \rightarrow 0_1)$	26.5242	26.3983	26.4811
	$B(E2; 2_2 \rightarrow 0_1)$	1.0640	1.1585	1.0411
	$B(E2; 2_3 \rightarrow 0_1)$	0.2563	0.2235	0.2299
	$B(E2; 2_2 \rightarrow 2_1)$	36.5153	36.4979	35.2698
	$B(E2; 2_3 \rightarrow 2_1)$	0.4322	0.2636	0.5776
System C	$B(M1; 1_1 \rightarrow 0_1)$	0.8160	0.8237	0.8007
	$B(M1; 1_1 \rightarrow 2_1)$	0	0	0
	$B(M1; 1_1 \rightarrow 2_2)$	1.0737	1.2676	1.0070
	$B(M1; 1_1 \rightarrow 2_3)$	0	0	0
	$B(E2; 1_1 \rightarrow 2_1)$	0.6158	0.5896	0.6109
	$B(E2; 1_1 \rightarrow 2_2)$	0	0	0
	$B(E2; 1_1 \rightarrow 2_3)$	44.8753	44.7753	46.8495
	$B(E2; 2_1 \rightarrow 0_1)$	21.3720	21.2188	20.9008
	$B(E2; 2_2 \rightarrow 0_1)$	0	0	0
	$B(E2; 2_3 \rightarrow 0_1)$	0.3677	0.3760	0.3461
	$B(E2; 2_2 \rightarrow 2_1)$	29.6375	29.2248	28.0001
	$B(E2; 2_3 \rightarrow 2_1)$	0	0	0

the γ -soft nucleus. Such an effectiveness of the axial PGCM is reconfirmed. Also, the validity of the $\gamma = 30^\circ$ intrinsic state is justified again.

Many properties derived from Table II are understood from the proton and neutron interacting boson model (IBM2). In the $O(6)$ dynamical symmetry limit of the IBM2, a strong $1_1 \rightarrow 2_2$ $M1$ decay is anticipated and the $1_1 \rightarrow 2_1$ $M1$ decay is strictly forbidden [21]. Conversely, the $1_1 \rightarrow 2_2$ $E2$ decay is forbidden and the $1_1 \rightarrow 2_1$ decay is predicted to have an $E2$ character in the $O(6)$ limit of the IBM2. These features can be seen in the two systems. Such characteristic EM properties have been reported in some γ -unstable nuclei [22–24].

For system C , the selection rules completely coincide with those in the $O(6)$ limit of the IBM2. We observe the vanishing $B(M1; 1_1 \rightarrow 2_3)$ and $B(E2; 2_3 \rightarrow 2_1)$ values as well as a strong $1_1 \rightarrow 2_3$ $E2$ transition. According to the IBM2, the $I_\kappa = 2_3$ state is interpreted as a mixed symmetry state. The strength of the $E2$ transition between the mixed symmetry and fully symmetric states is sensitive to the difference of the proton and neutron effective charges, $e_\pi - e_\nu$. We confirm that $B(E2; 2_3 \rightarrow 0_1)$ vanishes and $B(E2; 1_1 \rightarrow 2_3)$ is unchanged when we put $e_\pi = e_\nu = 1$. This validates the assignment of the $I_\kappa = 2_3$ state as a mixed symmetry state. The system B has a close resemblance to the system C , while strict selection rules do not hold true any longer. Remembering the fact that the triaxial deformation is essential for systems B and C , these consequences are not surprising.

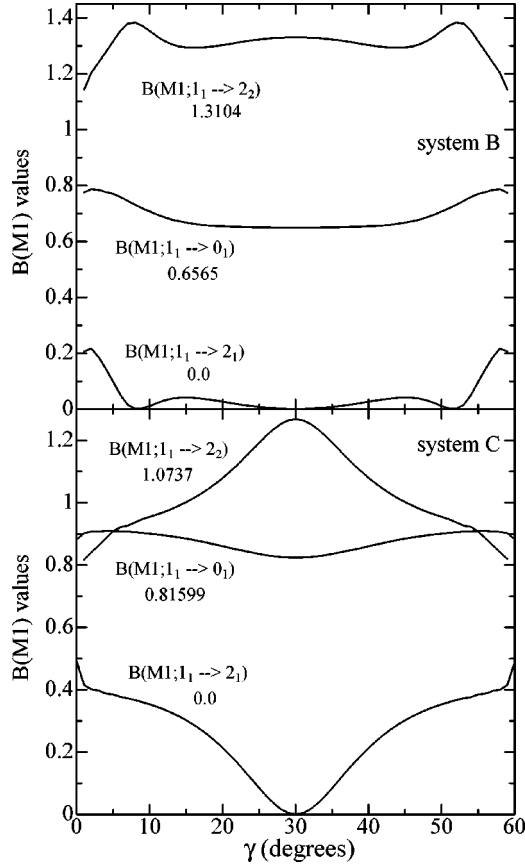


FIG. 11. $B(M1; 1_1 \rightarrow 0_1, 2_1, 2_2)$ values of systems *B* and *C* as functions of γ . The results correspond to those calculated in the triaxial PGCM subspace. For the sake of convenience, the exact $B(M1)$ values of the shell model calculation are shown in the figure.

Let us examine the γ dependence of the $B(M1)$ values in a manner similar to the PPES's. In Fig. 11, three $B(M1)$ values, i.e., $B(M1; 1_1 \rightarrow 0_1, 2_1, 2_2)$, are shown as functions of γ for systems *B* and *C*. We can draw some features common to two systems. As for the $M1$ transition from the scissors state to the ground state, the $B(M1)$ value calculated at $\gamma = 30^\circ$ gives the best description of the exact value as expected from the PPES's. The functional behavior of $B(M1; 1_1 \rightarrow 0_1)$ turns out to be similar to that of the PPES's of $I_\kappa = 0_1, 1_1$ (cf. Fig. 10). The large triaxial deformation is advantageous to produce the strong $M1$ decay from the scissors state to the $I_\kappa = 2_2$ quasi- γ band head. This view is applied more explicitly to system *C*, where the strength increases with triaxiality and reaches its maximum at $\gamma = 30^\circ$. The $B(M1)$ value at $\gamma = 30^\circ$ also accounts for the vanishing $1_1 \rightarrow 2_1$ decay. Its strength is small but nonzero for $\gamma \neq 30^\circ$.

With respect to the $E2$ transitions, we are interested in the γ dependence of $B(E2; 1_1 \rightarrow 2_1, 2_2)$. As mentioned above, the functional behavior of the two $E2$ transitions is strongly dependent on the choice of effective charges. An ambiguity arising from the effective charges is inevitable for the model

nucleus. Any $B(E2)$ value is always symmetric with respect to $\gamma = 30^\circ$ for system *C*. The same is true only in the case of $e_\pi = e_\nu$ for system *B*, and the $E2$ strength is stronger on the prolate side, if $e_\pi > e_\nu$. This is because system *B* is roughly regarded as a model nucleus made up of the prolate proton and oblate neutron bodies. The strong (weak) $1_1 \rightarrow 2_1(2_2)$ $E2$ decay is well reproduced, irrespective of γ . Also, the value of $B(E2; 1_1 \rightarrow 2_2)$ vanishes at $\gamma = 30^\circ$ for system *C*. However, as for the two $B(E2)$ values, physical information obtained from the γ dependence is not so rich as in the case of $E2$ transitions between symmetric states, e.g., $B(E2; 2_1, 2_2 \rightarrow 0_1)$ and $B(E2; 2_2 \rightarrow 2_1)$ [7].

The fundamental EM properties presented in this section are not strongly affected by the force parameter of the QQI, if $\chi_{\pi\pi}$ and $\chi_{\nu\nu}$ are not artificially large compared with $\chi_{\pi\nu}$.

VI. CONCLUSION

We have investigated various kinds of PGCM's on the basis of the proton-neutron single- j shell model. By using pure QQI, the quadrupole collectivity has been examined for three model nuclei.

We have begun our investigations from the standard PGCM, where the collective motion is described by the coherent motion of protons and neutrons. The results of the present work together with those in previous works [7–10] lead us to the conclusion that the correlations essential to the low-lying states can be correctly taken into account by the PGCM. Even for the p - n coupled system, its theoretical framework is reasonable as far as the p - n coherent motion is concerned.

In order to describe collective modes relevant to the p - n relative motion such as a scissors mode, we have extended the theoretical framework by explicitly separating the proton and neutron parts. We have proposed a truncation scheme by means of the PGCM. The truncation of the shell model has been carried out for three types of PGCM's, i.e., the simplest PGCM using a prolate intrinsic state, the axial PGCM, and the triaxial PGCM using a fixed intrinsic state. The merits and demerits of each truncation are transparent from its ingredients. A comparative study of respective truncations makes it easy to disclose collective contents hidden in the complicated band structure of the shell model. With small revision of the program code, we can perform many kinds of PGCM's for cross checking. This kind of flexibility is characteristic of the PGCM, and will be also useful for the analysis of real nuclei.

Along the lines of these investigations, we could clarify some properties of the model nuclei. For instance, the equilibrium deformation of the $I_\kappa = 1_1$ scissors state is found to be realized at $\gamma = 30^\circ$ for systems *B* and *C*. Namely, the PPES of the scissors state shows the triaxiality-favoring tendency similar to that of the ground state. As for the EM transition probabilities of the two triaxial model nuclei, the decay branches of the $I_\kappa = 1_1$ scissors state are similar to those predicted in the $O(6)$ limit of the IBM2.

- [1] K. Burzyński and J. Dobaczewski, *Phys. Rev. C* **51**, 1825 (1995).
- [2] N. Yoshinaga, T. Mizusaki, A. Arima, and Y. D. Devi, *Prog. Theor. Phys. Suppl.* **125**, 65 (1996).
- [3] S. S. Avancini, J. R. Marinelli, and D. P. Menezes, *J. Phys. G* **25**, 1829 (1999).
- [4] N. Yoshinaga, Y. D. Devi, and A. Arima, *Phys. Rev. C* **62**, 024309 (2000).
- [5] J. A. Sheikh and P. Ring, *Nucl. Phys.* **A665**, 71 (2000).
- [6] J. Dukelsky and S. Pittel, *Phys. Rev. C* **63**, 061303(R) (2001).
- [7] K. Enami, K. Tanabe, and N. Yoshinaga, *Phys. Rev. C* **63**, 044322 (2001), and references therein.
- [8] K. Enami, K. Tanabe, and N. Yoshinaga, *Phys. Rev. C* **64**, 044305 (2001).
- [9] K. Enami, K. Tanabe, and N. Yoshinaga, *Prog. Part. Nucl. Phys.* **46**, 177 (2001).
- [10] K. Enami, K. Tanabe, and N. Yoshinaga, *Czech. J. Phys.* **51**, A255 (2001).
- [11] M. Baranger and K. Kumar, *Nucl. Phys.* **62**, 113 (1965).
- [12] K. Enami, K. Tanabe, N. Yoshinaga, and K. Higashiyama, *Prog. Theor. Phys.* **104**, 757 (2000).
- [13] N. Lo Iudice and F. Palumbo, *Phys. Rev. Lett.* **41**, 1532 (1978).
- [14] F. Iachello, *Phys. Rev. Lett.* **53**, 1427 (1984).
- [15] D. Bohle, A. Richter, W. Steffen, A. E. L. Dieperink, N. Lo Iudice, F. Palumbo, and O. Scholten, *Phys. Lett.* **137B**, 27 (1984).
- [16] Y. Sun, C.-L. Wu, K. Bhatt, M. Guidry, and D. H. Feng, *Phys. Rev. Lett.* **80**, 672 (1998).
- [17] Y. M. Zhao, N. Yoshinaga, S. Yamaji, and A. Arima, *Phys. Rev. C* **62**, 014316 (2000).
- [18] J. P. Elliott, *Proc. R. Soc. London, Ser. A* **245**, 128 (1958); **245**, 562 (1958).
- [19] M. Harvey, *Adv. Nucl. Phys.* **1**, 67 (1968).
- [20] D. Rompf, T. Beuschel, J. P. Draayer, W. Scheid, and J. G. Hirsch, *Phys. Rev. C* **57**, 1703 (1998).
- [21] P. Van Isacker, K. Heyde, J. Jolie, and A. Sevrin, *Ann. Phys. (N.Y.)* **171**, 253 (1986).
- [22] P. von Brentano *et al.*, *Phys. Rev. Lett.* **76**, 2029 (1996).
- [23] H. Maser *et al.*, *Phys. Rev. C* **54**, R2129 (1996).
- [24] N. Pietralla *et al.*, *Phys. Rev. Lett.* **83**, 1303 (1999).